The Cryosphere Discuss., 9, 4355–4376, 2015
www.the-cryosphere-discuss.net/9/4355/2015/
doi:10.5194/tcd-9-4355-2015

The Cryosphere
Discussions
Open Access

Tilt error in cryospheric surface radiation measurements at high latitudes: a model study

W. S. Bogren[1,a], J. F. Burkhart[2,3], and A. Kylling[1]

[1]NILU – Norwegian Institute for Air Research, P.O. Box 100, 2027 Kjeller, Norway
[2]Department of Geosciences, University of Oslo, Oslo, Norway
[3]Sierra Nevada Research Institute, University of California, Merced, California, USA
[a]now at: NIBIO – Norwegian Institute of Bioeconomy Research, P.O. Box 115, 1431, Ås, Norway

Received: 17 June 2015 – Accepted: 31 July 2015 – Published: 18 August 2015

Correspondence to: J. F. Burkhart (john.burkhart@geo.uio.no)

Published by Copernicus Publications on behalf of the European Geosciences Union.

Abstract

We have evaluated the magnitude and makeup of error in cryospheric radiation observations due to small sensor misalignment in in-situ measurements of solar irradiance. This error is examined through simulation of diffuse and direct irradiance arriving at a detector with a cosine-response foreoptic. Emphasis is placed on assessing total error over the solar shortwave spectrum from 250 to 4500 nm, as well as supporting investigation over other relevant shortwave spectral ranges. The total measurement error introduced by sensor tilt is dominated by the direct component. For a typical high latitude albedo measurement with a solar zenith angle of 60°, a sensor tilted by 1, 3, and 5° can respectively introduce up to 2.6, 7.7, and 12.8 % error into the measured irradiance and similar errors in the derived albedo. Depending on the daily range of solar azimuth and zenith angles, significant measurement error can persist also in integrated daily irradiance and albedo.

1 Introduction

In situ observations of the albedo of snow-covered surfaces are important for a variety of purposes. As part of a manned measurement program or campaign, they allow high spectral resolution and correlation to physical properties of the snowpack (Aoki et al., 2000). When collected by an automatic weather station (AWS) or tower, albedo measurements contribute to a larger suite of energy balance and/or weather observations. In addition, in situ albedo measurement campaigns are necessary for validating remotely sensed observations of surface albedo (Stroeve et al., 1997; Liang, 2001; Klein and Stroeve, 2002) as well as improving and assessing results of climate models (Van Angelen et al., 2012).

The climate modeling community has previously called for an accuracy of 0.02 or better from albedo datasets used as model input (Sellers et al., 1995). Since ground

TCD
9, 4355–4376, 2015

measurements should be of higher accuracy than the datasets they validate, potential measurement errors of 0.01 or larger are significant and undesirable.

Error sources such as shading of the surface by the sensor setup, slope of the surface, accurate calibration of the sensors, and characterization of the sensor's angular response function are commonly recognized and addressed (e.g., Grenfell et al., 1994; Perovich et al., 2002; Gardner and Sharp, 2010; Nicolaus et al., 2010). The error due to tilting of the sensor is rarely discussed. In perhaps the most thorough uncertainty analysis of solar irradiance measurements, Bernhard and Seckmeyer (1999) estimated that the optics of an irradiance meter may be levelled to a standard uncertainty of $\pm 0.1^{\circ}$ resulting in 0.2 % uncertainty in the irradiance for a solar zenith angle of 60° and a wavelength of 400 nm. However, Stroeve et al. (2006) estimate the uncertainty in the AWS in situ albedo to be 0.035. The AWS instruments lack levelling certainty to reliably gauge sub-diurnal albedo variability and in the ablation zone levelling errors up to 40° have been experienced. Stroeve et al. (2001) acknowledge that "the primary source of error in the measurement of surface albedo is instrument level". However, they do not quantify this error for the instrument they use in their intercomparison between in situ and AVHRR derived surface albedo over Greenland. Other errors include imperfect cosine response, frost, and reflections/shadows.

In manned campaign settings, sensors are often removed from their mounting for safe transport to and from the measurement site. In order to achieve level irradiance measurements, the sensors must be mounted in proper orientation quickly and firmly, and the stand itself must be positioned and leveled with minimal disturbance to the snow pack beneath the sensors. For permanent installations, wind and changes in surface conditions (melting snow and ice) may change the sensor orientation. Achieving level measurement is even more difficult on a moving platform in turbulent conditions, such as a boat, ice buoy or small aircraft. Fortunately, such platforms often maintain an excellent record of orientation which can be used to assess uncertainty in irradiance and albedo measurements, and when necessary correct them to some degree.

TCD
9, 4355–4376, 2015

This study presents the first thorough quantification of the potential error in irradiance measurements from sensor orientation, considering separately the error in measured diffuse and direct irradiance, and the combined total error in tilted sensor measurements. The error is calculated by using a radiative transfer model to simulate the radiance field over a surface with a spectral albedo representative for snow. The radiance field is used together with an instrument levelling model to simulate the effect of levelling errors on measured irradiance as described in Sect. 2. The results from the simulations are presented in Sect. 3. In Sect. 4 we discuss the limitations and implications of these results, as well as recommendations for addressing this large source of measurement uncertainty. Conclusions are given in Sect. 5.

2 Methods

The surface albedo $A(\lambda)$ at wavelength λ is defined as the ratio between the upwelling, $E^{\uparrow}(\lambda)$ and downwelling, $E^{\downarrow}(\lambda)$, irradiances at the surface:

$$A(\lambda) = \frac{E^{\uparrow}(\lambda)}{E^{\downarrow}(\lambda)} \tag{1}$$

The global albedo A_g is defined as

$$A_g = \frac{\int_0^{\infty} E^{\uparrow}(\lambda)\mathrm{d}\lambda}{\int_0^{\infty} E^{\downarrow}(\lambda)\mathrm{d}\lambda}, \tag{2}$$

and the albedo measured by typical shortwave irradiance detectors

$$A_{SW} = \frac{\int_{250}^{2500} E^{\uparrow}(\lambda)\mathrm{d}\lambda}{\int_{250}^{2500} E^{\downarrow}(\lambda)\mathrm{d}\lambda}. \tag{3}$$

TCD
9, 4355–4376, 2015

Furthermore, we calculate the UV and visible albedo by integrating between 250 and 900 nm.

$$A_{vis} = \frac{\int_{250}^{900} E^{\uparrow}(\lambda)\mathrm{d}\lambda}{\int_{250}^{900} E^{\downarrow}(\lambda)\mathrm{d}\lambda}. \quad (4)$$

The daily integrated albedo is calculated following Stroeve et al. (2006)

$$A_i = \frac{\sum E^{\uparrow}}{\sum E^{\downarrow}}, \quad (5)$$

where the sum is over 24 h. Here and below we omit the λ dependence for simplicity, but, unless otherwise noted, it is implicitly included in all relevant quantities.

The upwelling and downwelling irradiances are defined as:

$$E^{\uparrow} = \int_0^{2\pi} \mathrm{d}\phi \int_{-\pi/2}^{0} L(\theta,\phi)\cos\theta\sin\theta\mathrm{d}\theta \quad (6)$$

$$E_{\mathrm{h}}^{\downarrow} = E_0^{\mathrm{sur}}\cos\theta_0 + \int_0^{2\pi} \mathrm{d}\phi \int_0^{\pi/2} L(\theta,\phi)\cos\theta\sin\theta\mathrm{d}\theta, \quad (7)$$

where $L(\theta,\phi)$ is the radiance for polar angle θ and azimuth angle ϕ and E_0^{sur} is the direct solar flux at the surface. The subscript h on $E_{\mathrm{h}}^{\downarrow}$ indicates that the irradiance is calculated with respect to the horizontal. Equation (1) implies a levelled instrument with perfect cosine response. For an un-levelled instrument the downwelling irradiance is

$$E_{\mathrm{t}}^{\downarrow} = E_0^{\mathrm{sur}}\cos(\theta_0 - \theta_{\mathrm{t}}\cos\phi_{\mathrm{t}}) + \int_0^{2\pi} \mathrm{d}\phi \int_{\Delta\theta}^{\pi/2+\Delta\theta} L(\theta,\phi)\cos\theta\sin\theta\mathrm{d}\theta \quad (8)$$

TCD
9, 4355–4376, 2015

where $\Delta\theta$ is the angle the instrument is tilted, thus the subscript t on E_t, and ϕ_t is the relative azimuth angle of the sensor tilt to the sun.

The difference between $E_h^{\downarrow}$ and $E_t^{\downarrow}$ will impact measurement of the albedo assuming negligible tilt error effect in $E^{\uparrow}$. To assess this impact, simulations of the radiance $L(\theta,\phi)$ were carried out for different solar angles and measurement geometries.

2.1 Radiative transfer model

The uvspec program from the libradtran software package (Mayer and Kylling, 2005) was used to simulate the radiance $L(\theta,\phi)$. Trace gas concentrations were taken from the subarctic summer atmospheric profile (Anderson et al., 1986). The surface was assumed to be Lambertian and a spectral surface albedo representative for pure snow was used (Wiscombe and Warren, 1980) unless otherwise noted. For global simulations the spectral resolution and dependence of trace gases were taken from the correlated-k distribution of Kato et al. (1999). For integration over shorter spectral intervals the Lowtran pseudo-spectral parameterisation (Ricchiazzi et al., 1998) was utilized. Clouds and aerosol were generally not included. Their impact is discussed in Sect. 3.4. The one-dimensional radiative transfer equation is solved by the DIScrete-Ordinate-method Radiative Transfer (DISORT) solver with 32 streams in pseudospherical geometry (Stamnes et al., 1988; Buras et al., 2011; Dahlback and Stamnes, 1991). The radiative transfer model computes both the direct and the multiple scattered diffuse radiation, $L(\theta,\phi)$. In these numerical experiments the angular resolution of the latter is at quarter degree resolution for both azimuth (θ) and polar (ϕ) angles.

2.2 Tilt calculation

The angres tool from the libradtran package was used to simulate the response of a tilted and rotated irradiance sensor. The angres tool takes as input a radiance field ($L(\theta,\phi)$) and an angular response function representing the instruments angular response. The integral in Eq. (8) is then performed for the tilted and rotated response

TCD
9, 4355–4376, 2015

function. The sensor was rotated from 0 to 180° relative azimuth at 2.5° intervals. The rotations were performed for sensor tilts of 1, 3, and 5°.

For all simulations the sensor angular response was modeled as a perfect cosine function, although it is well-known that real angular responses of irradiance meters do deviate from a true cosine response (Bais et al., 1998).

2.3 Sensitivity experiments

The simulations cover a range of solar zenith angles from noon (0°) to near-dusk (80°). As the majority of snow albedo measurements are made in polar regions, focus was on solar zenith angles greater than 50°.

Two sensitivity experiments were performed, aimed at quantifying sensitivity of the simulated error to constant surface albedo, and to the integrated spectral ranges. For the first experiment, the surface albedos of 0.9 and 0.2 were considered. For the second experiment, spectral integration was performed over wavelength bands chosen to match approximately the calibrated response of typical visible and complete shortwave irradiance detectors, covering respectively 250 to 900 nm and 250 to 2500 nm.

2.4 Analysis of sensor error

The total error introduced by a tilted sensor is the sum of the diffuse (η_{dif}) and direct errors (η_{dir}), each modified by their respective proportion of diffuse (P_{dif}) and direct (P_{dir}) irradiances ($P_{\text{dif}} + P_{\text{dir}} = 1$):

$$\eta = P_{\text{dir}}\eta_{\text{dir}} + P_{\text{dif}}\eta_{\text{dif}} \tag{9}$$

The sensor tilt error η is defined as the proportional difference between irradiance as measured by a tilted sensor, E_{t}, and the true irradiance on a horizontal surface, E_{h}:

$$\eta = \frac{E_{\text{t}} - E_{\text{h}}}{E_{\text{h}}} \tag{10}$$

TCD
9, 4355–4376, 2015

The cosine response of a level irradiance sensor is:

$$R(\theta)_{\mathrm{h}}^{\mathrm{dir}} = \cos\theta_0 \tag{11}$$

while the response of a sensor tilted θ_{t} degrees at ϕ degrees azimuth relative to the sun is:

$$R(\theta,\phi)_{\mathrm{t}}^{\mathrm{dir}} = \cos(\theta_0 - \theta_{\mathrm{t}}\cos\phi) \tag{12}$$

This is of similar form to Eq. (4) in Grenfell et al. (1994), which describes the error in measured albedo incurred when a horizontal measurement is taken over a sloping surface. The measurement error in direct irradiance, η_{dir}, is therefore insensitive to wavelength and can be calculated from the three variables: solar zenith angle θ_0, sensor tilt θ_{t}, and relative azimuth ϕ:

$$\eta_{\mathrm{dir}} = \frac{\cos(\theta_0 - \theta_{\mathrm{t}}\cos\phi) - \cos\theta_0}{\cos\theta_0} \tag{13}$$

The diffuse tilt error of the sensor η_{dif} was calculated, rightmost term Eq. (8), by integrating the tilted sensor angular response function across a diffuse radiance distribution and comparing with the result for the levelled sensor, rightmost term Eq. (7).

Finally, the analysis addresses the daily integration approach for "averaging out" measurement errors due to tilted sensors (Van den Broeke et al., 2004; Stroeve et al., 2006). Daily integrated measurements are simply the sum of irradiance measurements integrated over shorter intervals, for example five minutes, over a full day. In this analysis, solar radiation was modeled in 5 min intervals throughout the day. Irradiances for horizontal and tilted sensors were calculated for each of these solar orientations. Calculations were performed for a sensor tilted 3° at a fixed azimuth step, iterated around the compass to produce a full day of irradiance measurements. The error in the daily integrated irradiance is given by:

$$\eta = \frac{\sum E_{\mathrm{t}} - \sum E_{\mathrm{h}}}{\sum E_{\mathrm{h}}} \tag{14}$$

where it is summed over 24 h.

3 Results

We first discuss the significance of the diffuse error (η_{dif}). Next the proportion variables (P) are explored as functions of solar zenith angle (θ_{sun}) as well as wavelength, including an assessment of integrated visible and global spectra. The total error introduced by non-level sensor orientation is illustrated, in the form presented by Eq. (10). Sensitivity of modeled error to surface albedo and spectral range, as well as effectiveness of daily integration in reducing error are presented in their own subsections.

3.1 Diffuse component of sensor error: η_{dif}

The diffuse error varies with sensor tilt, relative azimuth, solar zenith angle, and wavelength. Figure 1 illustrates the global diffuse error η_{dif} for a sensor tilted 3°. The diffuse sensor error varies from 0.22 to 0.96 % for a 3° tilt, while a tilt of 1 and 5° have an error range of −0.05 to 0.19 % and 0.87 to 2.22 %, respectively. For all three tilt angles, variability within the reported range is a function of solar zenith angle and relative azimuth, following similar trends to those illustrated in Fig. 1. The diffuse error component is positive for all modeled orientations, meaning that the tilted sensor reports a higher value of diffuse irradiance than a levelled sensor. Increasing tilt or azimuth angle away from the sun results in a greater magnitude of error, while solar zenith angle has a variable affect.

3.2 Global error: incorporating P_{dir} and P_{dif}

The proportion of direct to diffuse irradiance as viewed by the sensor is also a function of tilt, relative azimuth, solar zenith angle, and wavelength. For all simulated cloudless cases for all solar and sensor orientations, the maximum value of the diffuse error term $P_{dif}\eta_{dif}$ is 0.35 % of the true irradiance. This is substantially less than the product of the

TCD
9, 4355–4376, 2015

maximum P_{dif} and the maximum η_{dif} because these two maxima do not occur at the same solar/sensor orientations.

Over the same range of solar/sensor orientations, the direct term $P_{dir}\eta_{dir}$ varies from 0 to 39.93 % of the true irradiance, with maximum magnitude of error at high solar zenith angle, high tilt, and sensors pointed either directly towards or away from the sun. The total sensor error, presented in Fig. 2, is therefore dominated by the direct term, and varies from 0 to 40.2 %.

3.3 Model sensitivity: spectral range

In order to test the spectral sensitivity of the modeled sensor error, three spectral ranges were investigated: the full solar spectrum (250–4500 nm), a pseudo-visible (250–900 nm) range; and a visible-infrared (250–2500 nm) range.

The diffuse error η_{dif}, not shown, does not vary dramatically between the simulated spectral ranges, and the direct error η_{dir} is insensitive to wavelength. Therefore variations in the proportional weighting factors P_{dif} and P_{dir} are the most significant difference between the three spectral ranges. As summarized in Table 1, the proportion of diffuse irradiance P_{dif} increases with higher tilt angles and shorter wavelengths.

3.4 Model sensitivity: surface albedo and homogeneous cloud cover

In order to test the model sensitivity to variations in surface albedo, the global calculations in Sect. 3.3, with Lambertian albedo of 0.9, was repeated with the value 0.2. The magnitude of the diffuse error decreases somewhat with lower albedo, but the most significant effect is once again the impact on the diffuse and direct proportional weighting factors, as summarized in Table 2 for P_{dir}. With higher P_{dir} over a low albedo surface, the global sensor error η_{glob} is higher. The maximum error η_{glob} for surface albedos of 0.2, 0.9, and pure snow albedo from Wiscombe and Warren (1980), are 40.2, 40.4, and 42.0 % respectively.

TCD
9, 4355–4376, 2015

Incorporating a layer of homogeneous ice clouds representative for conditions often found in high-albedo locations such as Summit, Grenland, and Antarctica, produced a similar result. While the effect on the diffuse and direct error terms was minimal, the tested cloud cover reduced global error by increasing the proportion of diffuse irradiance. These results are not presented here, as the values are entirely dependent on the definition of many separate parameters controlling the properties of the cloud cover.

3.5 Daily integrated irradiance

Error in daily integrated irradiance introduced by 3° sensor tilt was calculated for 6 days at Summit, Greenland, starting from solstice and continuing to mid-October. The results are valid for observations along the latitude 72.58°. The dates are chosen for the progression of solar zenith at local noon, from 49° (solstice) through 55, 60, 70, 75, and 80°.

As shown in Fig. 3, the potential error of the integrated measurements is highest when the sensor is tilted due north (0°) or due south (180°), and falls off when the pointing angle is closer to east or west. Within one month of solstice, the highest potential error in measured integrated irradiance remains under 1 %. However, measurements made more than two months from summer solstice by an automatic weather station tilted 3° due north or south show more than 5 % potential error in daily integrated irradiance.

4 Discussion

The potential error from sensor orientation has long been recognized (e.g., Van den Broeke et al., 2004; Stroeve et al., 2005), but methods for addressing the potential error are not often described in detail. The long-term instability of towers and weather stations deployed on ice sheets is well documented (e.g., Stroeve et al., 2005, 2006; Van de Wal et al., 2005). In validating MODIS albedo products, Stroeve et al. (2005,

2006) did not use AWS data when sensors were discovered during annual site visits to have levelling errors greater than 2° (Stroeve et al., 2005) and 3° (Stroeve et al., 2006); the resulting errors were addressed by using integrated daily albedo.

For realistic scenarios we have shown that the potential error in measured irradiance from a slight misalignment and levelling of the instrument may be greater than 2 %, and in some cases, much greater. However, the error varies over a broad range with the azimuth of the tilt, as well as variations in surface albedo and atmospheric conditions which can affect the proportions of diffuse and direct irradiances. It is not suggested that every measurement from a sensor which may have been tilted is subject to the maximum potential error; nor is it even suggested that existing measurements are too greatly influenced by this error to be useful. We do recommend greater care be placed into the levelling of measurements and feel hand leveled observations (e.g. on a hand held extension) are prone to larger errors than operators may expect.

Small levelling errors are extremely difficult to prevent when instruments are mounted on snow and ice. Accurate in situ measurements of albedo are important for validation of satellite products and input for climate models. For more recent applications such as attempting to estimate concentrations of aerosols and impurities deposited in the upper layer of a snowpack, it is critical that remaining sources of significant uncertainty are identified and addressed. Therefore, while existing measurements may or may not include components from this error source, it does represent a significant source of uncertainty that must be addressed for applications of albedo observations in polar regions.

With a precise record of sensor orientation, the potential error of a measurement can be estimated. However, sensors for monitoring orientation would add complications to design and deployment, especially for short term measurements. They are not typically integrated in the design of equipment for field campaigns, nor towers or automatic weather stations. Given the magnitude of potential error involved and the desired accuracy of measurements, this practice should be reconsidered. Knowledge of the sensor orientation may still not make it simple to fully correct the error unless a com-

TCD
9, 4355–4376, 2015

plete record of sky conditions is available, including ozone absorption in the UV, optical depths of significant aerosols, and single scattering albedo. For scattered clouds a 3-D radiative transfer model may be needed. Due to these challenges in applying accurate corrections, emphasis should be placed on recognizing the level of uncertainty introduced by a misaligned sensor, and taking every step to minimize errors in alignment. It is furthermore critical to maintain a precise log of sensor orientation in order to quantify firm boundaries on the uncertainty of a measurement. Potential errors due to tilt problems are also reduced by making measurements which integrate over short intervals close to noon, and for daily integrated values around summer solstice.

The results reported in this paper are for cloudless skies for which the impact of the tilt error is largest. It is also these measurement conditions that are used for satellite validation. Under cloudy or truly overcast skies, the ratio of diffuse irradiance will be higher, reducing the measurement error. However partially cloudy conditions could introduce higher values of η_{dif} than clear sky or complete overcast due to the sharp boundaries between bright clouds and dark sky, inducing more error when shifted over the cosine response function than a more gradually varying homogeneous sky.

5 Conclusions

Non-level irradiance measurements can result from a tilted or slowly shifting sensor installed over a snow surface or a rapidly shifting sensor mounted on a mobile platform. We have evaluated the error in irradiance measurements and corresponding albedo estimates due to sensor tilt, with a focus on high latitudes. The diffuse, η_{dif}, error due to the diffuse irradiance is of minimal importance as it is consistently low, varying between 0 and 2.2 % for all simulated geometries and model parameters. The total diffuse error term is further reduced to 0.35 % due to the proportion of diffuse and direct radiation, P_{dif}. By contrast the direct error, η_{dir}, varies from 0 to 50 %, reduced by direct proportion P_{dir} to a maximum 40 %. The simplest method for estimating sensor error is therefore $P_{\mathrm{dir}}\eta_{\mathrm{dir}}$, which deviates less than 0.35 % from the total sensor error for a clear polar atmosphere. The direct error η_{dir} can be calculated directly using Eq. (5) when the sensor and solar geometries are known, but P_{dir} must be measured or modeled.

The total error in irradiance and hence albedo measurements due to tilt errors, increase with increasing solar zenith angles. For a solar zenith angle of 60°, a sensor tilt of 1, 3, and 5° can introduce up to 2.6, 7.7, and 12.8 % error respectively, in the measured irradiance and derived albedo. The corresponding numbers for a solar zenith angle of 70° are 3.9, 11.8 and 19.6 %. Integrating measurements over the day decrease these numbers to a maximum of about ±4 % (10 %) for a tilt of 3° and solar zenith angle at noon of 60° (70°).

To correct measurements for tilt error is hard: at a minimum, for homogeneous skies, concurrent record of the diffuse/direct radiation ratio is required. For scattered clouds, a possibly prohibitive amount of measurements is needed in addition to 3-D radiative transfer modellling.

The present results demonstrate that tilt information is needed in order to improve the surface irradiance and albedo datasets used in climate studies and to validate satellite retrievals. Tilt information would make it possible to determine an upper bound for the measurement uncertainty due tilt error. Such uncertainty estimates due to tilt error should be included in the uncertainty estimates of the measured quantity.

Acknowledgement. This work was conducted within the Norwegian Research Council's NORKLIMA program under the Variability of Albedo Using Unmanned Aerial Vehicles (VAUUAV) project (NFR #184724) and The Remote Imaging and Spectral Characterization of the Cryosphere (RISCC) project (NFR #196204).

References

Anderson, G., Clough, S., Kneizys, F., Chetwynd, J., and Shettle, E.: AFGL atmospheric constituent profiles (0–120 km), Hansom AFB, Bedford, MA, 1986. 4360

Aoki, T., Aoki, T., Fukabori, M., Hachikubo, A., Tachibana, Y., and Nishio, F.: Effects of snow physical parameters on spectral albedo and bidirectional reflectance of snow surface, J. Geophys. Res., 105, 10219–10236, 2000. 4356

Augustine, J. A., DeLuisi, J. J., and Long, C. N.: Surfrad – a national surface radiation budget network for atmospheric resarch, B. Am. Meteorol. Soc., 81, 2341–2357, 2000.
Bais, A. F., Kazadzis, S., Balis, D., Zerefos, C. S., and Blumthaler, M.: Correcting global solar ultraviolet spectra recorded by a brewer spectroradiometer for its angular response error, Appl. Optics, 37, 6339–6444, 1998. 4361
Bernhard, G. and Seckmeyer, G.: Uncertainty of measurements of spectral solar UV irradiance, J. Geophys. Res., 104, 14321–14345, 1999. 4357
Buras, R., Dowling, T., and Emde, C.: New secondary-scattering correction in DISORT with increased efficiency for forward scattering, J. Quant. Spectrosc. Ra., 112, 2028–2034, doi:10.1016/j.jqsrt.2011.03.019, 2011. 4360
Dahlback, A. and Stamnes, K.: A new spherical model for computing the radiation field available for photolysis and heating at twilight, Planet. Space Sci., 39, 671–683, 1991. 4360
Gardner, A. S. and Sharp, M. J.: A review of snow and ice albedo and the development of a new physically based broadband albedo parameterization, J. Geophys. Res., 115, 1–15, doi:10.1029/2009JF001444, 2010. 4357
Grenfell, T. C., Warren, S. G., and Mullen, P. C.: Reflection of solar radiation by the Antarctic snow surface at ultraviolet, visible, and near-infrared wavelengths, J. Geophys. Res., 99, 18669–18684, 1994. 4357, 4362
Kato, S., Ackerman, T. P., Mather, J. H., and Clothiaux, E. E.: The k-distribution method and correlated-k approximation for a shortwave radiative transfer model, J. Quant. Spectrosc. Ra., 62, 109–121, doi:10.1016/S0022-4073(98)00075-2, 1999. 4360
Klein, A. G., and Stroeve, J.: Development and validation of a snow albedo algorithm for the MODIS instrument, Ann. Glaciol., 34, 45–52, doi:10.3189/172756402781817662, 2002. 4356
Liang, S.: Narrowband to broadband conversions of land surface albedo I Algorithms, Remote Sens. Environ., 76, 213–238, 2001. 4356
Mayer, B. and Kylling, A.: Technical note: The libRadtran software package for radiative transfer calculations - description and examples of use, Atmos. Chem. Phys., 5, 1855–1877, doi:10.5194/acp-5-1855-2005, 2005. 4360
Nicolaus, M., Hudson, S. R., Gerland, S., and Munderloh, K.: A modern concept for autonomous and continuous measurements of spectral albedo and transmittance of sea ice, Cold Reg. Sci. Technol., 62, 14–28, doi:10.1016/j.coldregions.2010.03.001, 2010. 4357

TCD
9, 4355–4376, 2015

Oerlemans, J. and Klok, E. J.: Energy balance of a glacier surface: analysis of automatic weather station data from the Morteratschgletscher, Switzerland, Arct. Antarct. Alp. Res., 34, 477–485, 2002.

Perovich, D. K., Grenfell, T. C., Light, B., and Hobbs, P. V.: Seasonal evolution of the albedo of multiyear Arctic sea ice, J. Geophys. Res., 107, 1–13, doi:10.1029/2000JC000438, 2002. 4357

Ricchiazzi, P., Yang, S., Gautier, C., and Sowle, D.: SBDART: a research and teaching software tool for plane-parallel radiative transfer in the Earth's atmosphere, B. Am. Meteorol. Soc., 79, 2101–2114, 1998. 4360

Sellers, P. J., Meeson, B. W., Hall, F. G., Asrar, G., Murphy, R. E., Schiffer, R. A., Bretherton, F. P., Dickinson, R. E., Ellingson, R. G., Field, C. B., Huemmrich, K. F., Justice, C. O., Melack, J. M., Roulet, N. T., Schimel, D. S., and Try, P. D.: Remote sensing of the land surface for studies of global change: models – algorithms – experiments, Remote Sens. Environ., 51, 3–26, 1995. 4356

Stamnes, K., Tsay, S.-C., Wiscombe, W., and Jayaweera, K.: Numerically stable algorithm for discrete–ordinate–method radiative transfer in multiple scattering and emitting layered media. Appl. Optics, 27, 2502–2509, 1988. 4360

Steffen, K. and Box, J.: Surface climatology of the Greenland ice sheet: Greenland climate network 1995–1999, J. Geophys. Res., 106, 33951–33964, 2001.

Stroeve, J.-C., Nolin, A., and Steffen, K.: Comparison of AVHRR-derived and in situ surface albedo over the Greenland Ice Sheet, Remote Sens. Environ., 62, 262–276, 1997. 4356

Stroeve, J.-C., Box, J. E., Fowler, C., Haran, T., and Key, J.: Intercomparison between in situ and AVHRR polar pathfinder-derived surface albedo over greenland, Remote Sens. Environ., 75, 360–374, 2001. 4357

Stroeve, J.-C., Box, J. E., Gao, F., Liang, S., Nolin, A., and Schaaf, C.: Accuracy assessment of the MODIS 16-day albedo product for snow: comparisons with Greenland in situ measurements, Remote Sens. Environ., 94, 46–60, 2005. 4365, 4366

Stroeve, J.-C., Box, J. E., and Haran, T.: Evaluation of the MODIS (MOD10A1) daily snow albedo product over the Greenland ice sheet, Remote Sens. Environ., 105, 155–171, doi:10.1016/j.rse.2006.06.009, 2006. 4357, 4359, 4362, 4365, 4366

van Angelen, J. H., Lenaerts, J. T. M., Lhermitte, S., Fettweis, X., Kuipers Munneke, P., van den Broeke, M. R., van Meijgaard, E., and Smeets, C. J. P. P.: Sensitivity of Greenland

Ice Sheet surface mass balance to surface albedo parameterization: a study with a regional climate model, The Cryosphere, 6, 1175–1186, doi:10.5194/tc-6-1175-2012, 2012. 4356

Van de Wal, R. S. W., Greuell, W., Van den Broeke, M. R., Reijmer, C. H., and Oerlemans, J.: Surface mass-balance observations and automatic weather station data along a transect near Kangerlussuaq, West Greenland, Ann. Glaciol., 42, 311–316, 2005. 4365

Van den Broeke, M., Van As, D., Reijmer, C., and Van de Wal, R.: Assessing and improving the quality of unattended radiation observations in Antarctica, J. Atmos. Ocean. Tech., 21, 1417–1431, doi:10.1175/1520-0426(2004)021<1417:AAITQO>2.0.CO;2, 2004. 4362, 4365

Wiscombe, W. J. and Warren, S. G.: A model for the spectral albedo of snow. I: Pure snow, J. Atmos. Sci., 37, 2712–2733, 1980. 4360, 4364, 4373

TCD

9, 4355–4376, 2015

Table 1. The diffuse proportion (P_{dif}) of global irradiance. Variability within the ranges presented is a function of sensor pointing azimuth as well as solar zenith angle. The simulations test a range of solar zenith angles from noon (0°) to near-dusk (80°), simulated in 5° steps.

Tilt	[250 to 4500 nm]	[250 to 2500 nm]	[250 to 900 nm]
1°	11.3–26.6 %	11.5–27.1 %	15.5–35.8 %
3°	11.4–31.8 %	11.6–32.3 %	15.5–41.7 %
5°	11.5–39.6 %	11.7–40.2 %	15.6–50.2 %

TCD
9, 4355–4376, 2015

Table 2. Diffuse proportion (P_{dif}) for different surface albedos. Variability within the ranges presented is a function of sensor pointing azimuth as well as solar zenith angle.

Tilt	Wiscombe and Warren (1980) clean snow	constant albedo 0.9	constant albedo 0.2
1°	12.0–27.1 %	11.3–26.6 %	5.4–22.0 %
3°	12.1–32.4 %	11.4–31.8 %	5.4–26.6 %
5°	12.1–40.3 %	11.5–39.6 %	5.4–33.6 %

TCD
9, 4355–4376, 2015

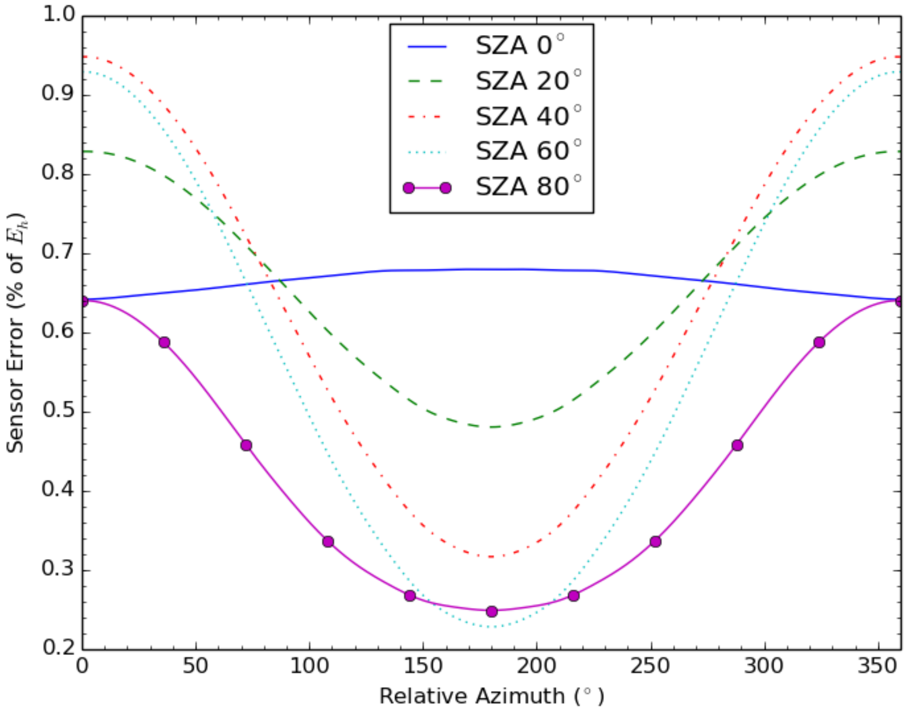

Figure 1. Simulated error in global diffuse irradiance, η_{dif}, for a cosine-response irradiance sensor tilted 3°.

TCD
9, 4355–4376, 2015

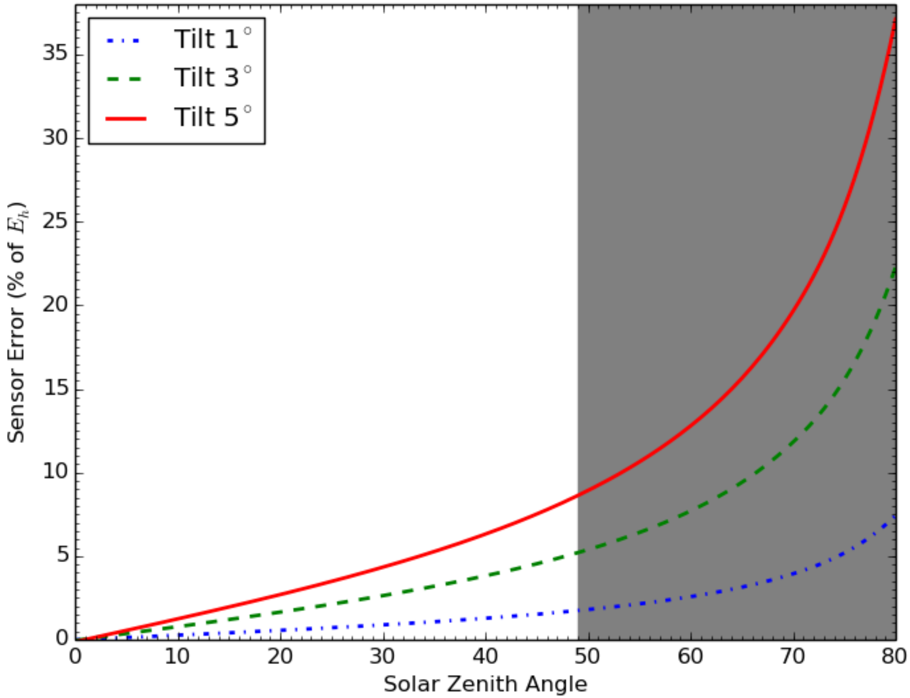

Figure 2. Total sensor error, η Eq. (9), for the full solar shortwave spectrum (global), for a sensor tilted directly toward the sun. The grey shaded area begins at 49°, representing the lowest observable solar zenith angle at Summit Station, Greenland (Latitude 72.58°).

TCD
9, 4355–4376, 2015

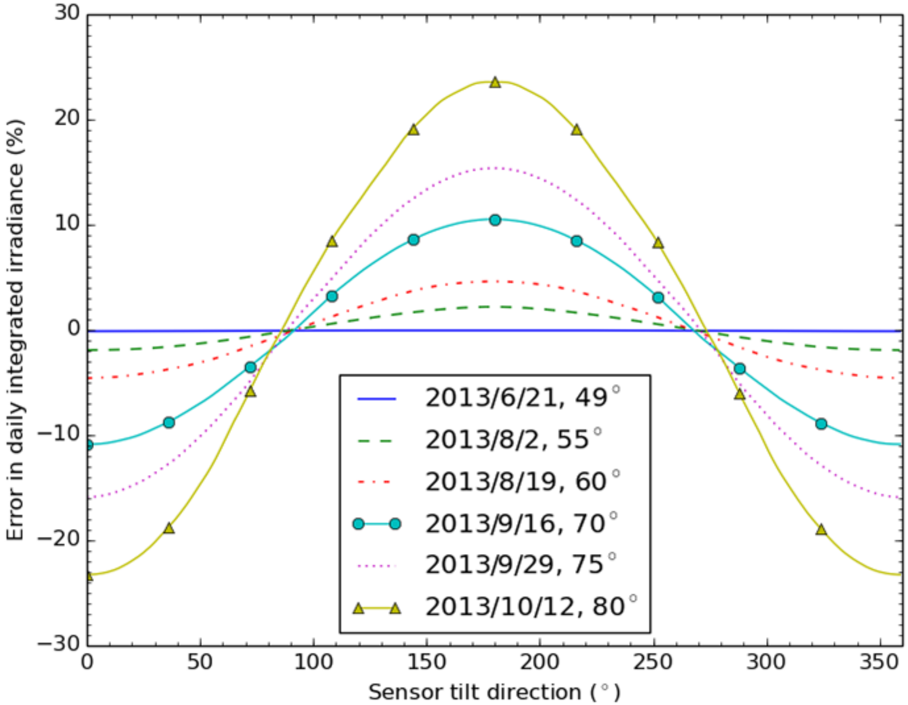

Figure 3. Error in daily integrated irradiance, Eq. (14), plotted against sensor tilt azimuth. Dates are chosen to show a local noon solar zenith angle of 49° (solstice), 55, 60, 70, 75, and 80° respectively, reading down the legend.

TCD
9, 4355–4376, 2015

Tilt error in cryospheric surface radiation measurements

W. S. Bogren et al.

Title Page
Abstract | Introduction
Conclusions | References
Tables | Figures
◄ | ►
Back | Close
Full Screen / Esc
Printer-friendly Version
Interactive Discussion